PNAS RESEARCH ARTICLE | EVOLUTION OPEN ACCESS

Evolution of genome-wide barriers to gene flow during complex speciation in rattlesnakes

Keaka Farleigh[a], Dylan K. Highland[a], Megan G. Alderman[a], Yannick Francioli[b], Samuel R. Hirst[c], Ellie M. Faber[a], Blair W. Perry[d], Matthew L. Holding[e,f], Gamaliel Castañeda-Gaytán[g], Miguel Borja[g], Hector Franz-Chávez[h], Christopher L. Parkinson[i], Jason L. Strickland[i], Mark J. Margres[c], Stephen P. Mackessy[k], Jesse M. Meik[l], Todd A. Castoe[b], and Drew R. Schield[a,1]

Affiliations are included on p. 11.

Edited by Marcus W. Feldman, Stanford University, Stanford, CA; received March 19, 2026; accepted April 27, 2026

Speciation with gene flow poses a central paradox: how do genome-wide barriers to gene exchange accumulate as recombination continually breaks down associations among selected loci? Although theory predicts that together recombination, selection, and genome structure shape reproductive isolation, empirical studies often report conflicting patterns, suggesting that these determinants change across the speciation continuum. Here we compare genomic landscapes of introgression across rattlesnake lineages spanning a range of divergence. We generated a chromosome-level reference genome for the Southwestern Speckled Rattlesnake (*Crotalus pyrrhus*) and analyzed whole genome data from 181 individuals across two species complexes with a history of gene flow upon secondary contact. We show that reproductive isolation is highly polygenic and dynamically structured. At early divergence, introgression is most reduced in high recombination regions, consistent with increased efficacy of selection against gene flow at few large-effect loci. As divergence progresses, linked selection against gene flow dominates, generating a positive relationship between recombination and introgression expected to occur through the genome-wide coupling of polygenic barrier effects. Introgression landscapes also become increasingly correlated across species pairs as divergence increases due to repeated evolution of barriers in the same genomic regions. Here, we infer that the Z chromosome plays a prominent role in reproductive isolation, harboring a disproportionate number of barrier loci and showing reduced introgression even at early divergence. Together, these results reveal how recombination, selection, and genome organization interact to shape speciation with gene flow upon secondary contact, reconciling empirical patterns with predictions of speciation theory.

barrier loci | gene flow | recombination | reproductive isolation | selection

Significance

How speciation occurs in the face of gene flow is a central question in biology. Comparing species at different stages of divergence enables us to better understand this process by tracing how barriers to gene exchange accumulate across the genome. Using genomic data from twelve rattlesnake species, we show that many genes contribute barriers to gene flow and that the strength of barrier effects is mediated by recombination rate as divergence progresses. Our data further support that the sex chromosomes contribute disproportionately to speciation in rattlesnakes, harboring a high density of loci putatively involved in hybrid incompatibilities and divergent ecological adaptation. Together, our findings illustrate how recombination and the buildup of genome-wide linkage disequilibrium shape transitions across the speciation continuum.

Understanding how barriers to gene flow evolve as populations diverge is central to our understanding of how new species originate (1). A key challenge is explaining how reproductive isolation emerges despite ongoing gene flow and recombination, which erode genetic associations among barriers to gene exchange. Because speciation proceeds as sources of reproductive isolation ("species barriers" or "barrier effects") and loci contributing to the overall reduction in gene flow ("barrier loci") accumulate (2–7), mapping the genomic landscape of species barriers can reveal the genetic architecture and evolution of reproductive isolation across the speciation continuum. At early stages of divergence, barriers to gene flow may be narrowly restricted to few loci underlying locally adapted traits with disproportionately large effects on hybrid fitness (2, 6, 8). As populations diverge, barrier loci become more widespread across the genome, resulting in fewer genomic regions where gene flow persists (6). Eventually, strong reproductive isolation is predicted to evolve through genomic coupling, the buildup of genome-wide linkage disequilibrium between polygenic barrier effects (7, 9), which enhances the total barrier to gene flow through the spread of indirect selection across barrier loci and nonbarrier loci [Fig. 1; (9–12)]. This framework therefore predicts a broad relationship between genetic divergence and the extent of reproductive isolation. Indeed, empirical studies have demonstrated lower rates of gene flow (or stronger reproductive isolation) between species pairs with greater genetic divergence in e.g., butterflies (13, 14), trees (15), and birds (16). Still, a major challenge in understanding the genomics of speciation is identifying where, why, and how rapidly barriers to gene flow accumulate across the genome (3), as their distribution and strength are shaped by genome organization, demographic history, geographic isolation, ecological divergence, and life history traits that influence both pre- and postzygotic isolation.

Author contributions: K.F. and D.R.S. designed research; K.F., D.K.H., M.G.A., Y.F., S.R.H., E.M.F., B.W.P., M.L.H., G.C.-G., M.B., H.F.-C., C.L.P., J.L.S., M.J.M., S.P.M., J.M.M., T.A.C., and D.R.S. performed research; M.J.M., S.P.M., J.M.M., T.A.C., and D.R.S. contributed new reagents/analytic tools; K.F., D.K.H., M.G.A., J.M.M., and D.R.S. analyzed data; and K.F. and D.R.S. wrote the paper.

The authors declare no competing interest.

This article is a PNAS Direct Submission.

[1]To whom correspondence may be addressed. Email: drew.schield@virginia.edu.

This article contains supporting information online at https://www.pnas.org/lookup/suppl/doi:10.1073/pnas.2609058123/-/DCSupplemental.

Published May 21, 2026.

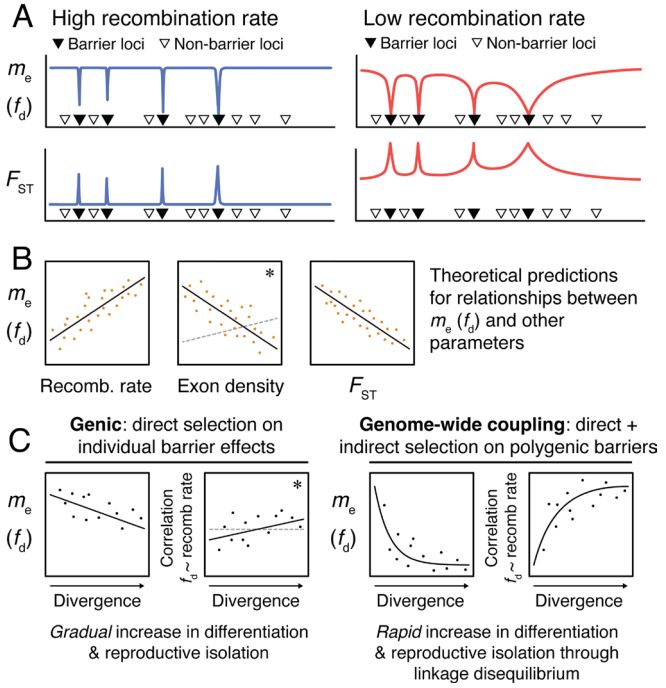

Fig. 1. Theoretical predictions for the evolution of genome-wide barriers to gene flow during complex speciation. (*A*) Reductions in effective migration rate (m_e), measured using f_d, at barrier loci contributing to reproductive isolation, adapted from Aeschbacher et al. (17). Under high recombination rate, reductions in m_e and associated increases in differentiation (F_{ST}) are localized to individual barriers and genome-wide F_{ST} is lower. Under low recombination rate, linkage between barrier loci and nonbarrier loci produces wider peaks of differentiation and higher genome-wide F_{ST} (although elevated F_{ST} can also result from processes unrelated to reproductive isolation). (*B*) Predicted relationships between rates of introgression and recombination rate, exon density, and F_{ST}. Points represent hypothetical data in genome scans. The asterisk and gray dashed line in the *Middle* panel reflect potential departures from the expected pattern due to the association between recombination and functional regions in snakes (18). (*C*) Predicted relationships between f_d and the strength of correlation between f_d ~ recombination rate and divergence time under models of individual "genic" barrier effects vs. genome-wide coupling of polygenic barrier effects. Points represent hypothetical data from pairs of species. When barriers are restricted to few uncoupled large-effect loci, direct selection is expected to produce gradual decreases in f_d as divergence increases. Correlations between f_d and recombination may increase with divergence, but the magnitude of this effect is uncertain (denoted by the asterisk and dashed gray line). Under genome-wide coupling, linkage disequilibrium strengthens the total barrier to gene flow through combined direct and indirect selection among barrier loci and nonbarrier loci (7, 9). Theory predicts that the buildup of genome-wide linkage disequilibrium during coupling may cause rapid transitions from weakly differentiated populations to strongly reproductively isolated species (12), denoted as a steeper nonlinear decrease in f_d with divergence. In turn, this process is expected to yield stronger correlations between f_d and recombination rate as divergence increases.

Despite the challenges of linking complex patterns of genetic differentiation to specific sources of reproductive isolation (particularly at later stages of the speciation process), theory and empirical evidence provide key predictions for where barriers will accumulate in the genome. For instance, barrier effects are likely to build up in genomic regions of low recombination due to selection against incompatible or maladaptive combinations of alleles in elevated linkage disequilibrium [Fig. 1*A*; (17, 19)]. By contrast, the effects of linked selection against foreign alleles will be reduced in regions with high recombination rate, resulting in these regions being more porous to gene flow (8). Together, these predictions imply that when reproductive isolation is polygenic, variation in rates of introgression should be positively correlated with recombination rate variation across the genome (Fig. 1 *B* and *C*). This pattern has been observed in butterflies (8), corn (20), fish (21), mice (22), and monkeyflowers (23). Alleles in coding and regulatory regions are most likely to experience direct selection against introgression (9, 24, 25), which predicts a negative genome-wide relationship between gene density and rates of introgression, as has been found in beeches (26), hominids (27), fungi (28), mice (29), and strawberries (30). Relatedly, regions affected by divergent selection may present strong barrier effects because admixture at these loci reduces hybrid fitness and thus contributes to reproductive isolation (31–34). However, studies often recover conflicting patterns across taxa and stages of divergence (e.g., refs. 8, 21, 22, 27, 35, and 36), suggesting that the genomic determinants of reproductive isolation are not static, but instead shift across the speciation continuum.

Moreover, the combined effects of recombination and adaptive differentiation on reproductive isolation may cause empirical observations to depart from theoretical expectations. In particular, interactions between recombination rate variation and the distribution of functional elements can obscure simple predictions based on either factor alone. For example, recombination rate is likely to strongly influence rates of gene flow in gene-dense regions (37). In humans, recombination rates are generally lower near genes (38), and there is a negative relationship between gene density and rates of gene flow (27). Similarly, *Heliconius* butterflies show reduced levels of admixture in gene-dense regions, which also have lower recombination rates (8). By contrast, recombination rates are elevated near functional regions in *Xiphophorus* swordtail fish (39), which also exhibit higher rates of introgression between species (21, 40). These findings highlight the need to evaluate how interactions between fine-scale recombination rate variation and the exposure of introgressed alleles to selection shape genetic divergence during speciation with gene flow. These contrasting patterns highlight a key unresolved question: are genomic barriers to introgression primarily structured by recombination rate, by gene density, or by their interaction—and does the answer depend on the stage and nature of divergence (i.e., divergent selection in the presence of gene flow vs. the accumulation of genetic incompatibilities in allopatry)?

A powerful approach to answering this question is to compare genomic landscapes of introgression between species across a continuum of divergence (41–43). Species pairs existing at different points along this continuum provide snapshots of the speciation process (Fig. 1*C*), allowing tests of whether genomic predictors of introgression change as divergence increases, and the degree to which patterns are replicated across lineages. This framework predicts that genome-wide relationships between recombination rate and introgression should strengthen as divergence increases and genome-wide coupling of barrier effects progresses, but will be weaker at earlier stages of the speciation continuum prior to the accumulation of polygenic barriers (8, 9, 11). Importantly, this approach enables empirical tests of whether the strength of the total barrier to gene flow (inversely proportional to m_e in Fig. 1*C*) increases linearly across the speciation continuum through individual barrier effects, or instead exhibits sharp transitions consistent with the combined effects of direct and indirect selection through genome-wide coupling (6, 7, 9, 11, 12).

Rattlesnakes (genus *Crotalus*) provide an exceptional opportunity to disentangle how genomic patterns of introgression change across the speciation continuum. This system combines complex speciation between lineages of varying divergence with distinctive genome organization, enabling comparative tests rarely possible within a single clade. Previous studies demonstrate that gene flow in secondary contact has been prevalent during rattlesnake diversification throughout the Pliocene and Pleistocene (44–49), with the presence of known hybrid zones (50–55) and broad evidence of introgression even between deeply divergent species [(56–59); *SI Appendix*]. Distinctive aspects of genome organization and recombination rate

variation in snakes may strongly influence patterns of introgression. Snake genomes are composed of both macrochromosomes and microchromosomes, which differ considerably in structure and composition, including a combination of higher recombination rates and higher gene density on microchromosomes than macrochromosomes (18, 60). At finer scales, recombination rate variation is shaped by a combination of PRMD9 binding and localization of recombination hotspots to functional regions, resulting in a genome-wide effect of elevated recombination rates in genes and promoter-like features (18, 61). Last, rattlesnake species exhibit substantial variation in aspects of morphology, physiology, and ecology despite widespread signatures of gene flow between divergent populations and species. This includes interspecific and intraspecific variation in seasonality, body size, reproductive strategies, cryptic coloration, and venom composition evolved in response to diverse intrinsic and extrinsic selection pressures (49, 62–66). Accordingly, divergent selection due to local adaptation is likely a key source of reproductive isolation.

Here, we study genomic introgression within the Speckled and Western Rattlesnake species complexes to evaluate how recombination, selection, and genome organization jointly shape barriers to gene flow across a continuum of divergent parapatric and sympatric species pairs. By integrating comparative introgression landscapes with patterns of fine-scale recombination rate and genomic features, we test whether the determinants of reproductive isolation change predictably across the speciation continuum (Fig. 1), and whether the same genomic regions repeatedly contribute to species barriers in secondary contact.

Results

Genome Assembly, Annotation, and Variant Calling. We sequenced and assembled a chromosome-level genome from a male Southwestern Speckled Rattlesnake (*Crotalus pyrrhus*) as a reference for our analyses (Fig. 2*A*). The total assembly is 1.6 Gbp in length and is highly contiguous and complete, with a contig N50 of 93.16 Mbp, scaffold N50 of 206.8 Mbp, and 98.43% BUSCO completeness (*SI Appendix*, Table S1). The assembly includes individual scaffolds representing each of the 17 autosomes (seven large macrochromosomes and 10 microchromosomes under 30 Mbp) and the Z chromosome, which we identified based on chromosomal synteny with *Crotalus viridis* (60) and *Crotalus adamanteus* (67). Our genome annotation includes 19,217 protein-coding genes and indicates that 51% of the genome is composed of repetitive elements (*SI Appendix*, Table S2). Whole genome sequencing and variant calling resulted in 49,644,347 SNPs for analysis. Our dataset consists of 181 individuals (Fig. 2*B*), including five species within the Western Rattlesnake species complex, five species within the Speckled Rattlesnake species complex, and two outgroup species (*SI Appendix*, Table S3).

Phylogeny, Population Structure, and Historical Demography. We resolved phylogenetic relationships within the Speckled and Western Rattlesnake species complexes and established a temporal framework for evolutionary divergence using coalescent species tree, concatenated maximum-likelihood, and phylogenetic network approaches (Fig. 2 *C* and *D* and *SI Appendix*, Figs. S1 and S2). All approaches support reciprocal monophyly of the two species complexes, which diverged from a common ancestor approximately 4.8 MYA. *Crotalus tigris* is strongly supported as sister to the Speckled Rattlesnake complex sensu stricto, with an estimated divergence of ~4.2 MYA, followed by diversification within the Speckled complex from the Late Pliocene through the Pleistocene. Relationships within the Speckled complex recover paraphyly of *C. pyrrhus* with respect to *Crotalus mitchellii*, with multiple geographically structured lineages (Fig. 2*C*), consistent with earlier phylogenetic hypotheses (46, 68). Within the Western complex, *C. viridis* diverged from remaining species approximately 3.1 MYA, followed by Mid-Pleistocene separation of "Pacific" (*Crotalus oreganus, Crotalus helleri*) and "Intermontane" (*Crotalus lutosus*, *Crotalus concolor*) clades (18, 69). Phylogenetic network analyses reveal multiple reticulation events within and between species complexes, consistent with a history of introgression during diversification [Fig. 2*D*; (46, 49, 58, 59, 69, 70)]. Analyses of population structure (ADMIXTURE and PCA; *SI Appendix*, Figs. S1, S3 and S4) recapitulate phylogenetic relationships while indicating admixture in several species. Demographic estimates indicate substantial variation in current N_e among species (i.e., 6,000 to 900,000), with most species undergoing expansion or contraction events since the Late Pleistocene (*SI Appendix*, Fig. S5); see details in *SI Appendix*.

Genomic Landscapes Reveal Patterns of Introgression in *Crotalus*. We measured introgression within and between the two species complexes using the summary statistic f_d (71), which leverages the ABBA-BABA framework (72) to quantify estimates proportional to the effective migration rate based on inferred "admixture proportions" (8, 71). Higher f_d values can be interpreted as elevated effective migration rates, whereas an f_d of zero indicates no signal of introgression. We also performed analyses of linkage disequilibrium and sequence divergence to test the possibility that f_d patterns reflect variable rates of incomplete lineage sorting alone, but do not find evidence in support of this hypothesis. These patterns instead support the presence of gene flow in secondary contact, consistent with previous analyses (*SI Appendix*). Genome-wide f_d varies widely among the 13 parapatric and sympatric species pairs analyzed (Fig. 3 and *SI Appendix*, Figs. S6 and S7 and Table S4), spanning an order of magnitude between the lowest and highest estimates (mean ± SD f_d= 0.015 ± 0.02 between *C. pyrrhus* and *C. tigris*; f_d= 0.245 ± 0.14 between *C. oreganus* and *C. helleri*). Genome-wide f_d estimates therefore confirm the presence of gene flow during diversification (e.g., refs. 49, 58, and 59), with substantial variation in rates of introgression between species.

Genomic landscapes of introgression are highly heterogeneous, exhibiting fine-scale variation in "peaks" and "valleys" of f_d within and among chromosomes for each pair of species (Fig. 3 and *SI Appendix*, Fig. S7). This is especially apparent for species with higher genome-wide f_d (e.g., *C. oreganus* and *C. helleri*, *C. viridis* and *C. concolor*, and *C. pyrrhus* and *C. stephensi*), which show a "sawtooth" pattern due to comparatively high-magnitude differences in f_d between potential barrier loci and regions porous to gene flow. Within chromosomes, f_d is consistently elevated between species in telomeric regions, most notably at the end of Chromosome 2 and start of Chromosome 4 (*SI Appendix*, Fig. S7). Admixture proportions also tend to be highest on microchromosomes, intermediate on macrochromosomes, and lowest on the Z chromosome, with significant differences in f_d distributions between chromosome types (*SI Appendix*, Fig. S8 and Table S5; Mann–Whitney U tests). This pattern of relative introgression across chromosomes is largely consistent among species pairs, except for species with shallow genetic divergence (e.g., *C. oreganus* and *C. helleri*, *C. lutosus*, and *C. concolor*). Departures in these species are not consistently statistically significant (*SI Appendix*, Table S5), though interestingly, recently diverged *C. oreganus* and *C. helleri* show the opposite pattern from most species, with higher f_d on macrochromosomes and the Z chromosome than microchromosomes (P-values = 0.007 and 0.011, respectively). The substantial heterogeneity in admixture between *Crotalus* species is consistent with variable selection against gene flow at many loci across the genome (i.e., polygenic species barriers), which we examine in detail below.

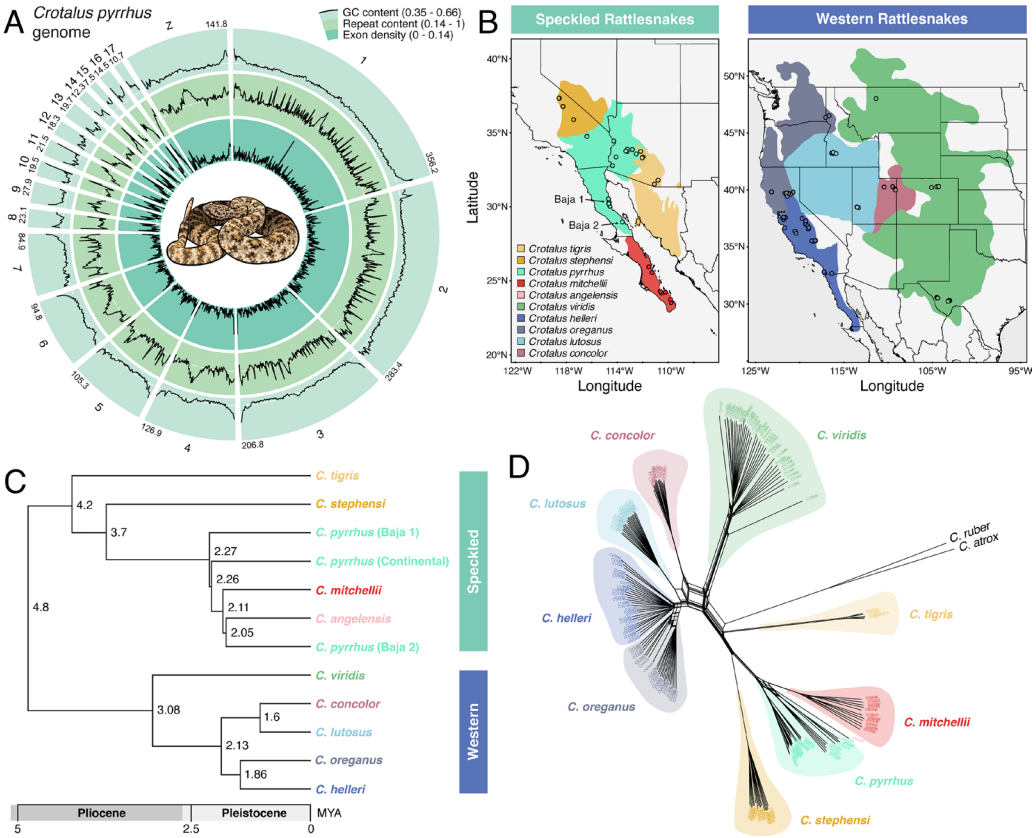

Fig. 2. Genome assembly and study system. (*A*) Genome structure and composition across the chromosome-level Southwestern Speckled Rattlesnake (*C. pyrrhus*) genome assembly. Black lines show variation in GC content (*Outer*), repeat content (*Middle*), and exon density (*Inner*). Chromosome names and total lengths (Mbp) are labeled. (*B*) Geographic distributions of the Speckled Rattlesnake (*Left*) and Western Rattlesnake (*Right*) species complexes. Sampling localities are indicated by circles on the maps. (*C*) Estimated species tree topology and divergence times for the two species complexes. Node labels indicate mean divergence time in millions of years (MYA). (*D*) Phylogenetic network showing relationships among all samples, with reticulations indicated by parallel lines at ancestral nodes.

Recombination Rate Variation Shapes Polygenic Barriers to Gene Flow. We next tested theoretical predictions for how the accumulation of species barriers across the rattlesnake genome is shaped by recombination and selection (Fig. 1). First, we calculated correlation coefficients between f_d and recombination rate, exon density, and genetic differentiation (F_{ST}; *SI Appendix*, Table S6). We find significant positive correlations between f_d and recombination rate in nine of the 13 species pairs (Fig. 4 and *SI Appendix*, Figs. S9 and S10; Spearman correlation coefficients, P-values $< 2.2 \times 10^{-16}$), the strongest of these being between recombination rate and f_d in *C. pyrrhus* and *C. stephensi* ($\rho = 0.4$) and the weakest being f_d in *C. mitchellii* and *C. helleri* ($\rho = 0.22$). Species pairs with shallow genetic divergence were the only exceptions to this more general pattern; we find a significant negative correlation between f_d and recombination rate in *C. oreganus* and *C. helleri* (Fig. 4 and *SI Appendix*, Fig. S9; $\rho = -0.25$, P-value $< 2.2 \times 10^{-16}$), while f_d between *C. oreganus* and *C. lutosus*, *C. lutosus* and *C. concolor*, and *C. oreganus* and *C. viridis* show no significant relationship with recombination rate (*SI Appendix*, Fig. S9). Interestingly, f_d is weakly positively correlated with exon density in most species (Fig. 4 and *SI Appendix*, Fig. S11, $\rho = 0.08$ to 0.2). Weakly negative or nonsignificant correlations with exon density occur in the same species pairs as above for recombination rate. While the sign and significance of relationships between f_d and recombination rate and exon density change as a function of divergence between species, f_d and F_{ST} are consistently negatively correlated between all species pairs (Fig. 4 and *SI Appendix*, Fig. S12; $\rho = -0.29$ to -0.63, P-value $< 2.2 \times 10^{-16}$). This result is expected to some degree, because F_{ST} is influenced by within-population genetic diversity and should therefore decrease under higher effective migration rates (73, 74). On the other hand, negative relationships between genetic differentiation and admixture may also hint at reproductive isolation due to local adaptation to different environments, with high F_{ST} reflecting strong divergent selection relative to gene flow (32).

Weak positive relationships between rates of introgression and exon density are intriguing because they run counter to the prediction that the strength of barriers to gene flow depends on the density of targets of selection (19, 22, 25). However, two key features of meiotic recombination in snakes may help to explain this pattern. First, previous studies demonstrate that recombination rate is strikingly nonuniform across the genome, instead being concentrated in 1 to 2 kb recombination "hotspots" (18, 61). Second, recombination hotspots are often associated with functional regions, driving higher recombination rates in regions of high gene density (18). In light of these features, we performed additional analyses to disentangle the effects of recombination rate and exon density on introgression. We identified recombination hotspots in the *C. pyrrhus* genome as narrow regions with >5 × relative recombination rate when compared to 20 kb upstream and downstream flanking regions (Fig. 5*A* and *SI Appendix*, Table S7). Hotspots are on average 1,068 bp in length and have a mean relative rate of >30 × at center, with precipitous declines in recombination rate within several kilobases. Recombination rates are also elevated near genes (Fig. 5*B*), recapitulating findings in *C. viridis* and *C. oreganus* (18). We find that f_d is significantly higher in recombination hotspots than coldspots for 10 species pairs (Mann–Whitney U tests, P-values $\leq 4.9 \times 10^{-4}$; see Fig. 5*C* for example results in *C. pyrrhus* and *C. stephensi*; full results are shown in *SI Appendix*, Table S8). Similarly, f_d is significantly higher in genic regions than intergenic regions for the same species (Fig. 5*C* and *SI Appendix*, Table S9; P-values $\leq 8 \times 10^{-3}$); *C. oreganus* and *C. helleri* are the only species pair showing significant opposite trends, and we find no significant differences between regions for *C. oreganus* and *C. lutosus* and for *C. lutosus* and *C. concolor*.

Looking to the relative effects of recombination and exon density on introgression, partial redundancy analysis indicates that recombination rate explains higher proportions of genome-wide variance in f_d than exon density (*SI Appendix*, Table S10), and multiple linear

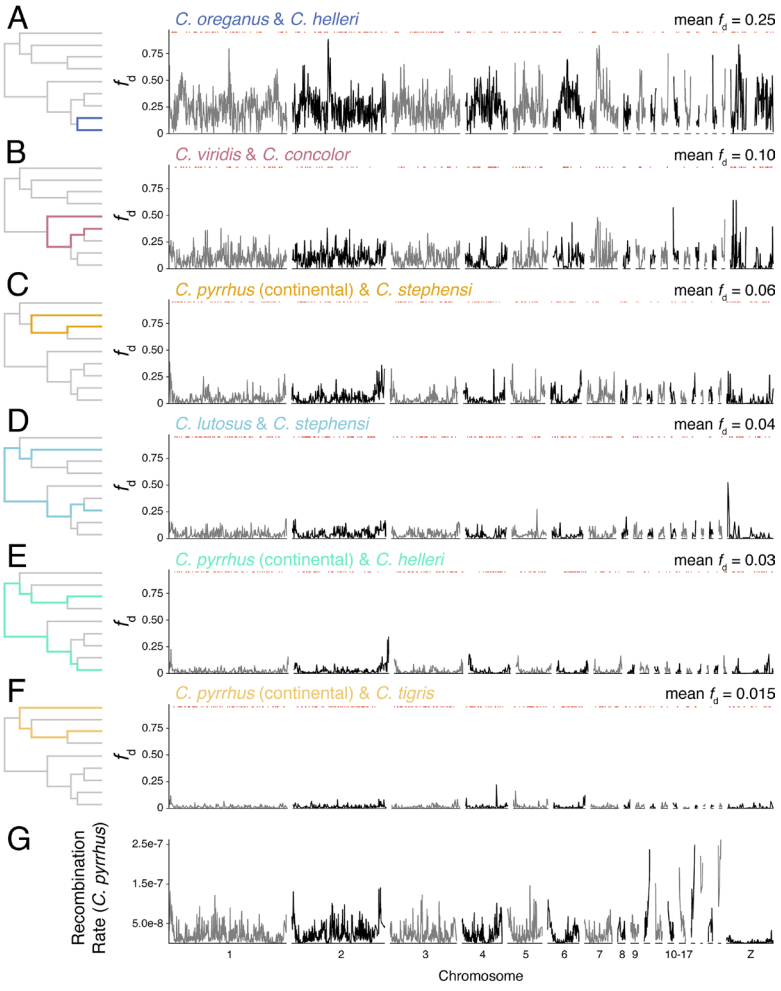

Fig. 3. Genomic landscapes of introgression between *Crotalus* species, illustrated by genome scans of admixture proportions (f_d) between *C. oreganus* and *C. helleri* (*A*), *C. viridis* and *C. concolor* (*B*), *C. pyrrhus* and *Crotalus stephensi* (*C*), *C. lutosus* and *C. stephensi* (*D*), *C. pyrrhus* and *C. helleri* (*E*), and *C. pyrrhus* and *C. tigris* (*F*). Genome scans (*Right* panels) show mean f_d in 1 Mb windows with a 100 kb step between windows; results for all species comparisons are shown in *SI Appendix*, Fig. S7. Genome-wide mean f_d for each comparison is indicated at the *Top Right*. Red dots above scans show locations of inferred barrier loci, as determined by permutation tests. (*G*) Recombination rate variation in *C. pyrrhus*. Shaded branches in trees to the *Left* of f_d scans highlight the phylogenetic distance between pairs of species.

regression shows a negative interaction effect of recombination rate and exon density on f_d in eight of 13 species pairs (*SI Appendix*, Table S11). Similar to genome-wide relationships between introgression and recombination rate, f_d is significantly positively correlated with recombination rate in hotspot regions, specifically, for most species (Fig. 5*D* and *SI Appendix*, Fig. S13 and Table S12). By contrast, there is no correlation between f_d and exon density in any species pair when we control for recombination rate in, and distance to, the nearest hotspot (Fig. 5*D* and *SI Appendix*, Fig. S13 and Table S13; multiple linear regression, *P*-values $\geq$ 0.052). Together, our data support the conclusion that rates of introgression are primarily shaped by recombination rate variation, and that genome-wide relationships between f_d and exon density (Fig. 4 and *SI Appendix*, Fig. S11) are a consequence of elevated recombination rates in functional regions. More broadly, genome-wide correlations between admixture and recombination rate support the hypothesis that species barriers are polygenic, with a higher proportion of loci contributing barrier effects in regions of low recombination than elsewhere in the genome.

Accumulation of Species Barriers Across Scales of Divergence. We next leveraged comparisons across all species pairs to examine the accumulation of barriers to gene exchange across a continuum of evolutionary and ecological divergence. As described above, very closely related species show distinct patterns from the majority of species pairs (Fig. 4 and *SI Appendix*, Figs. S9–S12), consistent with a hypothesized tipping point during divergence at which barrier effects accumulate more rapidly across the genome [Fig. 1; (35, 75, 76)]. We tested this hypothesis by examining the sign and strength of genome-wide correlations between f_d and recombination rate as a function of evolutionary divergence between species (proportional to divergence time). We find a significant quadratic relationship between $\rho(f_d \sim \text{rate})$ and evolutionary divergence across species (Fig. 6*A*; $R^2 = 0.81$; a linear model was rejected by AICc, *SI Appendix*, Table S14). There are two notable features of this relationship. First, the model slope is maximal at early to intermediate stages of divergence, with a rapid shift from the significant negative correlation in *C. oreganus* and *C. helleri* to significant positive correlations exemplified by most species pairs (*SI Appendix*, Fig. S9). Second, the relationship weakens at more advanced stages of divergence, suggesting that reproductive isolation has built up to the extent that barrier loci are less restricted to low recombination regions of the genome. Relatedly, there is a significant exponential decrease in mean genome-wide f_d with evolutionary divergence (Fig. 6*B*; $R^2 = 0.57$; *SI Appendix*, Table S14). These patterns are consistent when corrected for phylogenetic nonindependence (*SI Appendix*, Fig. S14). Together, these findings are consistent with an increase in the total barrier to gene flow across the speciation continuum through genome-wide coupling of polygenic barrier effects (Fig. 1*C*).

We also examined relationships between introgression and ecological divergence to test the hypothesis that divergent selection between environments promotes reproductive isolation. We developed a composite measure of ecological divergence between species based on ecological niche, breeding seasonality, and morphological data (*Materials and Methods*); this is a coarse measure, but nonetheless reflects key axes of rattlesnake variation subject to divergent

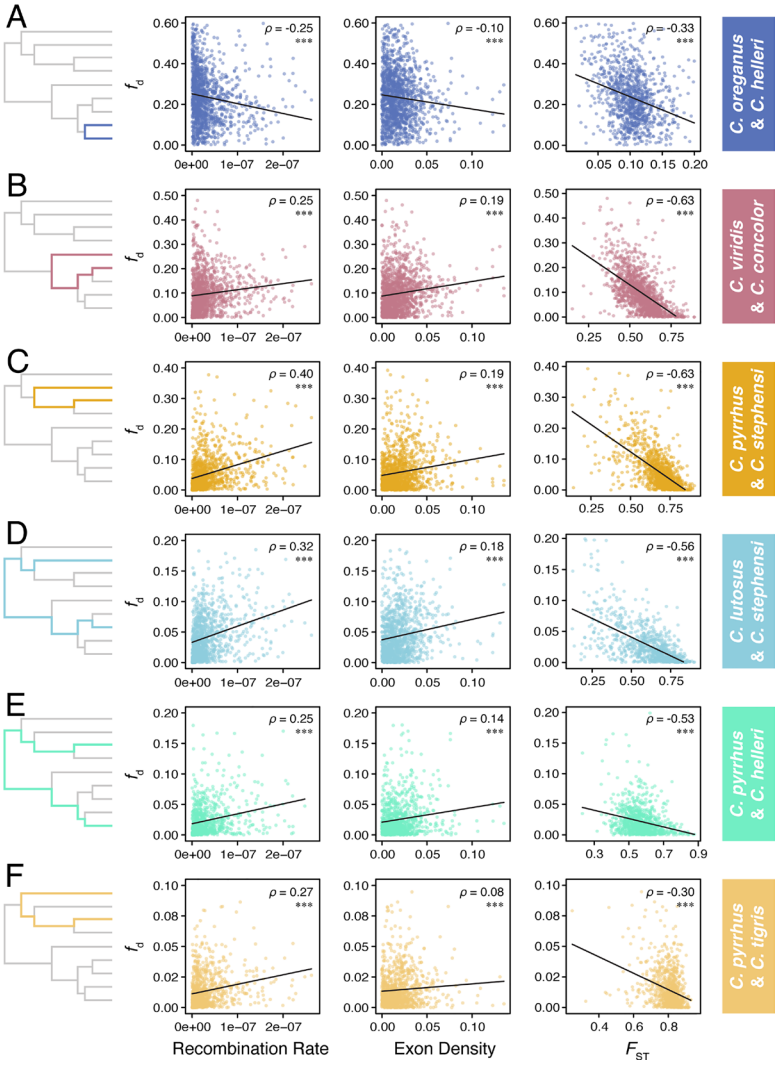

Fig. 4. Relationships between genomic landscapes of introgression and other parameters across scales of divergence, illustrated by *C. oreganus* and *C. helleri* (*A*), *C. viridis* and *C. concolor* (*B*), *C. pyrrhus* and *C. stephensi* (*C*), *C. lutosus* and *C. stephensi* (*D*), *C. pyrrhus* and *C. helleri* (*E*), and *C. pyrrhus* and *C. tigris* (*F*). Results for all species comparisons are shown in *SI Appendix*, Figs. S9–S12. Shaded branches in trees to the *Left* highlight the phylogenetic distance between species pairs. Panels from *Left* to *Right* show relationships between admixture proportion (f_d) and recombination rate, exon density, and F_{ST}, respectively, with labels for Spearman correlation coefficients (ρ) and significance ($^{***}P < 2.2 \times 10^{-16}$). All statistical comparisons are based on mean values in nonoverlapping 1 Mb windows.

selection (46, 54, 55, 77–82). We find a significant negative correlation between f_d and ecological divergence (Fig. 6*C*; Spearman correlation, $\rho = -0.71$, P-value = 0.02; *SI Appendix*, Table S14). This relationship suggests an increase in the total barrier to gene flow as the ecology of two species becomes more distinct, a precise prediction under a scenario of isolation-by-adaptation (32, 83). An alternative explanation could be that reduced migration rates are driven by spatial separation if ecological divergence correlates with geographic distance, yet we find no significant correlation between these variables (Spearman correlation, $\rho = 0.15$, P-value = 0.62). Tests comparing pairwise genetic divergence and ecological divergence further support isolation-by-adaptation. Absolute genetic divergence (d_{xy}), which is unaffected by variation in N_e within populations, is significantly positively correlated with ecological divergence (*SI Appendix*, Fig. S15*A*; Spearman correlation, $\rho = 0.57$, P-value = 0.04). Relative genetic differentiation (F_{ST}), which is sensitive to within-population N_e, also shows a positive, albeit nonsignificant, relationship with ecological divergence (*SI Appendix*, Fig. S15*B*; $\rho = 0.19$, P-value = 0.13).

Composition of Species Barriers and Links to Prezygotic and Postzygotic Isolation. We have shown that genomic landscapes of introgression in *Crotalus* become more tightly associated with recombination rate variation as divergence progresses (Figs. 4–6 and *SI Appendix*, Fig. S9). This pattern, together with broad-scale conservation of recombination landscapes [*SI Appendix*, Figs. S10 and S16; (18, 50)], raises the question of whether certain genomic regions repeatedly contribute to barrier effects between different species. We first tested for broad evidence of shared landscapes of barrier effects by quantifying correlations of f_d measured in 1 Mb windows between independent species pairs (e.g., *C. pyrrhus* and *C. tigris* vs. *C. viridis* and *C. concolor*). After correcting for multiple-testing, we find that 28 of 45 total pairwise comparisons are positively correlated (Spearman correlations, $\rho = 0.072$ to 0.268, P-values $\leq$ 0.047), whereas three comparisons are negatively correlated ($\rho = -0.134$ to -0.16, P-values $< 7.26 \times 10^{-5}$) and 14 comparisons show no significant correlation (Fig. 6*D* and *SI Appendix*, Table S15). Correlation coefficients for pairs of f_d landscapes increase with evolutionary divergence, regardless of whether the minimum divergence or mean divergence between species pairs is used as the predictor variable (Fig. 6*D*; *SI Appendix*, Fig. S17; $\rho_{(\text{min div})} = 0.74$, P-value $< 4.4 \times 10^{-4}$; $\rho_{(\text{mean div})} = 0.43$, P-value = 0.02). This pattern also holds when corrected for phylogenetic nonindependence (*SI Appendix*, Fig. S18). These findings support the hypothesis that genomic landscapes of introgression become more similar with increasing genetic divergence due to the repeated accumulation of barrier effects in the same genomic regions.

For detailed investigation of barrier loci and their composition, we identified outlier 1 Mb windows with extremely low f_d in each pair of species relative to null distributions generated using permutations (*Materials and Methods*). As inferred from relationships between recombination and admixture described above, barrier

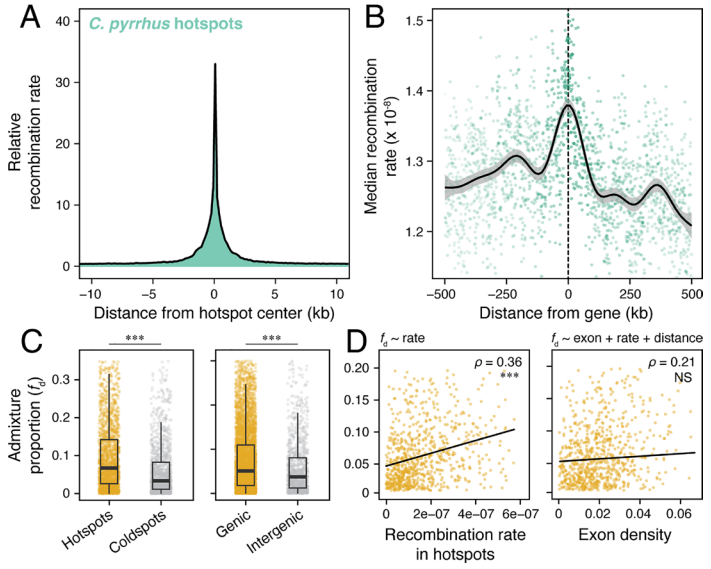

Fig. 5. Barriers to introgression are shaped by recombination rate variation. (*A*) Relative rates in recombination hotspots annotated in the *C. pyrrhus* genome. Relative rates were calculated by dividing recombination rates in hotspot centers by rates in the surrounding 40 kb regions. (*B*) Recombination rate in 500 kb upstream and downstream regions of genes. Points depict median recombination rates in 500 bp nonoverlapping windows, with darker points indicating higher numbers of observations. The black line and gray shaded area represent a loess smoothed average and 95% CI, respectively. (*C*) Admixture proportions (f_d) between *C. pyrrhus* and *C. stephensi* in recombination hotspots and coldspots (*Left*) and genic and intergenic regions (*Right*), with significance of Mann–Whitney ∪ tests shown above. (*D*) Relationships between f_d and mean recombination rate in hotspot windows (*Left*) and between f_d and exon density in hotspot windows, while controlling for recombination rate in the nearest hotspot and the distance (in bp) to the nearest hotspot (*Right*). Formulas of each linear model are shown above, and Spearman correlation coefficients are summarized in the *Top Right* of each panel. Results for all species comparisons are provided in *SI Appendix*, Tables S8–S13. Results from comparisons with species-specific recombination rates are in *SI Appendix*, Fig. S13. Shaded points in (*C*) and (*D*) represent mean values in nonoverlapping 100 kb windows overlapping each feature. In all panels, $^{***}P < 2.2 \times 10^{-16}$; NS, not significant.

windows tend to fall in regions with low recombination rate (*SI Appendix*, Table S16) and are genomically widespread (Fig. 3 and *SI Appendix*, Fig. S7), appearing across all chromosomes between nearly all species. Barriers also show a substantial degree of overlap; of 1,215 distinct barrier windows identified across the 13 species pairs, 794 (65%) occur in at least two pairs. Shared barrier windows appear in 37% of species pairs on average, higher than a maximum of 26% expected by random chance in simulations (Fig. 6*E*), even when controlling for recombination rate (*SI Appendix*, Fig. S19 and *Materials and Methods*) and after phylogenetic correction. Moreover, 549 shared barrier windows are identified in species pairs exceeding this simulated threshold (i.e., four species pairs), 73 are identified in eight or more pairs, and five barrier windows are detected in all species. Shared barrier windows contain a total of 5,290 genes. We performed functional analysis of genes in barrier regions using gene ontology assignments to assess whether polygenic species barriers relate to specific sources of reproductive isolation. Numerous biological processes are indeed significantly overrepresented after correcting for multiple comparisons (Fig. 6*E* and Dataset S1), including related functional categories with putative links to prezygotic and postzygotic isolation. Among these, overrepresentation of genes involved in chemosensory behavior (five genes, *P*-value = 0.015) and related terms raises the intriguing possibility that divergent selection on chemosensory repertoires promotes prezygotic isolation through mate discrimination. We also find 26 genes in barrier windows involved in fertilization (*P*-value = 0.017), supporting that postmating prezygotic isolation is a relevant mechanism of speciation in rattlesnakes. Many other overrepresented functional categories relate to key aspects of reproduction, homeostasis, and mitochondrial function, including oogenesis (13 genes, *P*-value = 0.011), spermatogenesis (90 genes, *P*-value = 0.011), embryo development (174 genes; *P*-value = 5.68×10^{-28}), regulation of type-2 mitophagy (five genes, *P*-value = 0.0014), and regulation of oxidative phosphorylation (seven genes, *P*-value = 0.0169). Functional categories putatively linked to compensatory evolution

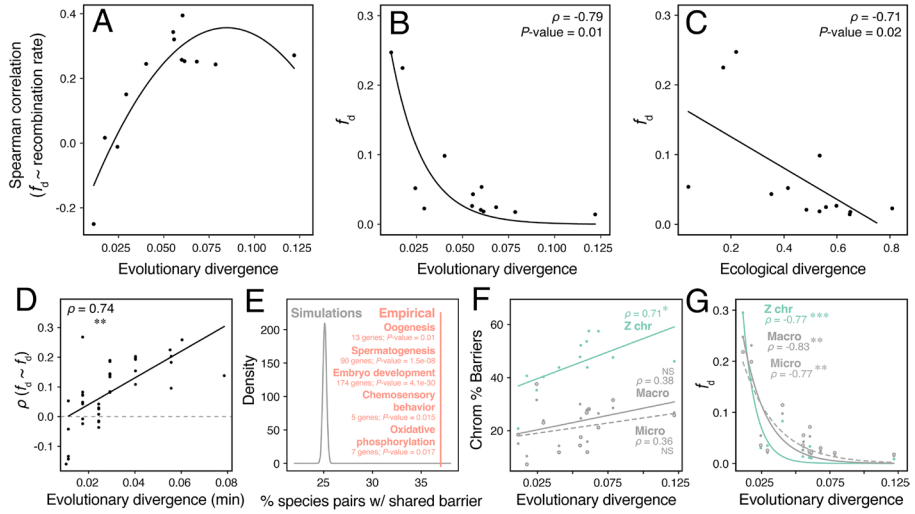

Fig. 6. Genome-wide barriers accumulate with evolutionary and ecological divergence between species. (*A*) Spearman correlation coefficients between admixture proportions (f_d) and recombination rate as a function of evolutionary divergence. Points are drawn from correlation coefficients calculated from measures in 1 Mb nonoverlapping windows (Fig. 4 and *SI Appendix*, Fig. S9). (*B*) Relationship between mean genome-wide f_d and evolutionary divergence. (*C*) Relationship between mean genome-wide f_d and ecological divergence. Labels in *A* and *B* summarize Spearman correlation coefficients between f_d and evolutionary and ecological divergence, respectively. Lines in (*A–C*) represent best-fit nonlinear or linear models to the data. (*D*) Spearman correlation coefficients (ρ) for genome-wide admixture proportions (f_d) between all species pairs as a function of the minimum evolutionary divergence in each set of species pairs, calculated based on mean f_d in nonoverlapping 1 Mb windows. (*E*) Simulated distribution (gray) of the proportion of species pairs sharing a coincident barrier window identified in any given pair of species, compared to the empirical mean (vertical salmon line). Overrepresented biological processes within shared barrier windows relevant to pre- and postzygotic isolation are labeled, along with numbers of associated genes. (*F*) Relationships between the proportion of chromosomes identified as barrier windows and evolutionary divergence between species, with results shown separately for macrochromosomes (closed gray points; solid gray line), microchromosomes (open gray points; dashed gray line), and the Z chromosome (green points; green line). (*G*) Relationship between mean f_d and evolutionary divergence, with results shown separately for macrochromosomes (closed gray points; solid gray line), microchromosomes (open gray points; dashed gray line), and the Z chromosome (green points; green line). In all panels, $^{***}P < 2.2 \times 10^{-16}$; $^{**}P < 0.001$; $^{*}P < 0.05$; NS, not significant.

with venom are also overrepresented in barrier regions (Dataset S1; e.g., response to toxic substance, 29 genes, P-value = 0.0089; venom-mediated blood coagulation, five genes, P-value = 0.029).

Considering the accumulation of species barriers at a broader scale, we mapped the proportions of chromosomes comprised of outlier barrier windows as a function of evolutionary divergence between species. Autosomes show positive but nonsignificant trends (Fig. 6*F*), with similar proportions of barrier windows seen across macrochromosomes and microchromosomes across scales of divergence (albeit with slightly lower proportions on microchromosomes, which have higher recombination rates on average). By contrast, the Z chromosome is highly enriched for shared barrier windows among species (Fisher's exact tests; *SI Appendix*, Table S17), as evidenced by a higher intercept in the linear model relative to autosomes and statistical comparison of proportions of barrier windows among chromosome types (Kruskal–Wallis test, $P\text{-value}_{(\text{Z vs micro})} = 3.8 \times 10^{-5}$, $P\text{-value}_{(\text{Z vs macro})} = 3.8 \times 10^{-5}$, $P\text{-value}_{(\text{micro vs macro})} = 0.4$). The proportion of Z chromosome constituting barriers also increases significantly as divergence increases (Fig. 6*F*; Spearman correlation, $\rho = 0.71$, P-value = 0.03). Consequently, rates of introgression decay more rapidly on the Z chromosome than autosomes and at earlier stages of divergence (Fig. 6*G*; Z decay rate = −105.98, macro = 57.54, micro = −40.62; Z inflection point = 0.035, macro = 0.055; micro = 0.06). This pattern also holds when comparing the Z chromosome to the autosome most similar in length (Chromosome 4; *SI Appendix*, Fig. S20). These results support the presence of "large Z-effects" (84, 85) in rattlesnake speciation in the presence of gene flow, which we discuss below.

Candidate Genes Illustrate Interplay Between Selection and Introgression. As a complement to broad characterization of genes in barrier windows, we examined fine-scale patterns of introgression in genes underlying venom and adaptive immunity, traits with known fitness functions and well-characterized genetic architectures (56, 60, 67, 86–88). Venom genes exhibit significantly elevated f_d relative to genome background distributions between multiple species pairs (e.g., *C. pyrrhus* and *C. stephensi*, *C. pyrrhus* and *C. tigris*, and *C. viridis* and *C. concolor*; Fig. 7 *A* and *B* and *SI Appendix*, Table S18). Fig. 7 shows f_d scans for exemplar species pairs to illustrate patterns in two major venom gene regions, the snake venom metalloproteinases (SVMP) and snake venom serine proteases (SVSP). We focus on these species because they allow us to compare signals of introgression across scales of divergence within the Speckled Rattlesnake complex (*C. pyrrhus* and *C. stephensi*), within the Western Rattlesnake complex (*C. oreganus* and *C. helleri*), and between the species complexes (*C. pyrrhus* and *C. helleri*). There are localized f_d peaks in the SVMP region between each of these species pairs (Fig. 7*A*). Here, admixture is substantially elevated between both *C. pyrrhus* and *C. stephensi* and *C. pyrrhus* and *C. helleri*, roughly 7 × to over 10 × higher than median f_d across the entire chromosome. While comparatively modest, relative f_d between *C. oreganus* and *C. helleri* in the SVMP region is also notable given that these species share much higher levels of genome-wide admixture. We also find a substantial f_d peak between *C. pyrrhus* and *C. stephensi* in the SVSP region (Fig. 7*B*), reflecting higher overall rates of venom introgression within the Speckled Rattlesnakes (*SI Appendix*, Table S18).

Rates of introgression are significantly elevated in major histocompatibility complex (MHC) genes relative to background distributions in eight of 13 species pairs (*SI Appendix*, Table S19), potentially facilitated by balancing selection favoring the persistence of allelic diversity (though balancing selection will also delay lineage sorting, generally). The remaining species pairs show no significant difference in f_d between MHC genes and the genome background (i.e., no species show reduced in introgression at these loci). As in the SVMP venom gene region, we find locally elevated f_d between multiple species in the MHC Class II region on Chromosome 2 (Fig. 7*C*), including a broad region of admixture between *C. pyrrhus* and *C. stephensi* and a highly concentrated peak of admixture between *C. pyrrhus* and *C. helleri*, in which f_d is 17 × higher than the chromosomal median. Recombination rates are also significantly elevated in venom and MHC regions relative to barrier windows (*SI Appendix*, Fig. S21; Mann–Whitney ∪ test; P-value = 0.0003).

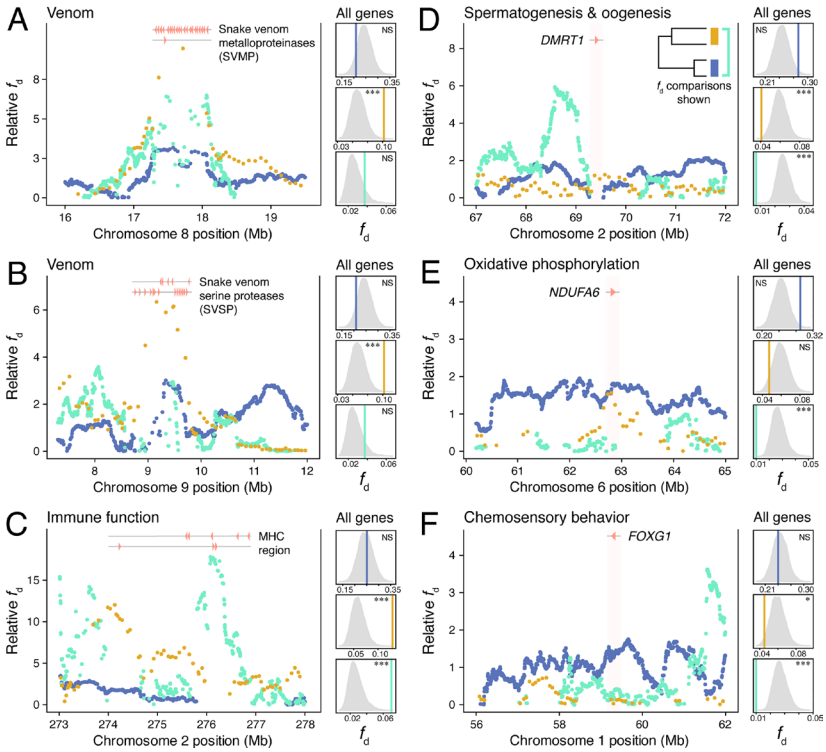

Fig. 7. Signatures of introgression at focal genes linked to fitness and reproductive isolation illustrate the interplay between selection and gene flow during speciation. (*A*) Venom: snake venom metalloproteinases (SVMP); (*B*) Venom: snake venom serine proteases (SVSP); (*C*) Immune function: major histocompatibility complex (MHC) Class II region; (*D*) Spermatogenesis and oogenesis: *DMRT1* locus; (*E*) Oxidative phosphorylation: *NDUFA6* locus; (*F*) Chemosensory behavior: *FOXG1* locus. *Left* panels in (*A*–*F*) show f_d scans at focal gene regions between exemplar species pairs at different stages of divergence: within the Western Rattlesnake complex (blue; *C. oreganus* and *C. helleri*), within the Speckled Rattlesnake complex (orange; *C. pyrrhus* and *C. stephensi*), and between the species complexes (green; *C. pyrrhus* and *C. helleri*); illustrated by tree *Inset* in *D*. Genes are shown as salmon arrows. *Right* panels in *A*–*F* show comparisons between median f_d among all genes in each category (blue, orange, and green vertical lines) and simulated null distributions (gray). Labels summarize results of Mann–Whitney ∪ tests. In all panels, $^{***}P < 2.2 \times 10^{-16}$; $^{*}P < 0.05$; NS, not significant.

In contrast to venom and MHC loci, fine-scale patterns at candidate genes linked to functional categories overrepresented in barrier windows (Fig. 6*E* and Dataset S1) demonstrate evidence for selection against gene flow. Analysis of f_d in genes involved in oogenesis and spermatogenesis, embryo development, oxidative phosphorylation, and chemosensory behavior support significantly reduced rates of introgression between most species relative to genome background distributions (Fig. 7 *D–F* and *SI Appendix*, Tables S20–S23). Individual candidate genes also exhibit localized reductions in f_d between one or more of our exemplar species pairs. For example, *DMRT1*, which plays critical roles in sex differentiation and spermatogenesis, shows punctuated decreases in relative f_d between *C. pyrrhus* and *C. helleri* and between *C. oreganus* and *C. helleri* (Fig. 7*D*). While the nuclear-encoded mitochondrial gene *NDUFA6* shows similar rates of introgression within the respective species complexes to the genome background, f_d is substantially reduced between *C. pyrrhus* and *C. helleri* (Fig. 7*E*). Last, *FOXG1*, which is involved in development of the vertebrate chemosensory system, shows locally reduced f_d between both *C. pyrrhus* and *C. stephensi* and *C. pyrrhus* and *C. helleri* (Fig. 7*F*). Together, comparisons between loci with known fitness functions and putative barrier loci illustrate variable selection for and against gene flow during speciation.

Discussion

Explaining how genome-wide barriers to gene flow emerge and accumulate as divergence proceeds in the presence of recombination between populations remains a persistent challenge, as few empirical studies have traced this process across the speciation continuum. We addressed this limitation by mapping genomic landscapes of introgression between rattlesnake species spanning a continuum of divergence, revealing patterns consistent with major transitions in the genetic architecture of reproductive isolation during speciation with gene flow upon secondary contact. Barriers to gene flow in *Crotalus* are polygenic and the effect of recombination on the genomic distribution of species barriers strengthens with divergence, supporting that the buildup of genome-wide linkage disequilibrium between barrier effects [i.e., genome-wide coupling; (7, 9)] is a key factor in the transition from differentiated populations to reproductively isolated species.

Whereas species barriers are restricted to few large-effect loci under direct selection at the onset of divergence (34, 89–91), the relative effects of indirect selection are predicted to spread through the coupling of polygenic barrier effects as divergence proceeds (7, 12, 92). During this phase of speciation, even loci with weak individual effects can collectively generate strong reproductive isolation when statistical associations among barriers are maintained by linkage disequilibrium, despite ongoing recombination (9, 11, 75). Theoretical models predict that divergent selection at a threshold number of loci can cause rapid transitions toward the completion of speciation through genome-wide coupling, wherein the entire genome acts as a cohesive barrier [Fig. 1; (11, 12, 76)]. However, empirical demonstrations of these transitions are lacking because they require that gene flow is measured for multiple taxon pairs across a continuum of divergence (12).

Comparative analyses across the Speckled and Western Rattlesnake species complexes bring key empirical data to bear on this body of theory. Rates of introgression vary dramatically across scales of divergence (Figs. 2 and 3 and *SI Appendix*, Figs. S6 and S7), and genome-wide relationships between introgression and recombination rate support that hitchhiking effects contribute to the spread of reproductive isolation through linkage disequilibrium and indirect selection (75, 91, 93). These relationships strengthen as divergence increases, as do relationships between introgression landscapes of independent species pairs (Fig. 6). Species at intermediate scales of divergence exhibit genome-wide structuring of introgression, characterized by heterogeneity in admixture and strong associations between introgression and recombination rate. By contrast, introgression landscapes are weakly structured at earlier stages of divergence, consistent with selection acting on relatively few loci of large-effect prior to the emergence of coupled barrier effects, facilitating introgression even in regions with low recombination rate. Finally, rates of introgression decay exponentially rather than gradually with divergence time, illustrating the predicted transition from genic to "genomic" phases of complex speciation through genome-wide coupling [Fig. 1; (7, 9, 12)]. Evidence for divergence-dependent coupling of species barriers helps to reconcile why empirical relationships between recombination rate and introgression vary across taxa and stages of divergence, while underscoring the need for comparative analyses spanning the speciation continuum to discover emergent genomic properties underlying the evolution of reproductive isolation.

The presence of polygenic barriers suggests that epistasis contributes to the buildup of reproductive isolation, particularly as complex genetic incompatibilities have arisen with time [i.e., "snowball' effects"; (6, 94–97)]. Although epistasis is not strictly necessary for genome-wide coupling (11), the presence of barriers at interacting genes underlying key biological processes suggests a role of epistasis in maintaining strong reproductive isolation upon secondary contact in *Crotalus*. Indeed, species barriers are repeatedly associated with genes involved in spermatogenesis, oogenesis, embryogenesis, and oxidative phosphorylation (Figs. 7 and 8 and Dataset S1), implicating the disruption of reproduction and mitonuclear coevolution through hybrid incompatibilities as recurrent sources of postzygotic isolation. These signatures align with prior studies of rattlesnake hybrid zones (50, 53) and predictions that divergence at these loci is especially likely to reduce hybrid fertility or viability (97–100).

We also find evidence that divergent ecological selection contributes to reduced gene flow between species. Effective migration rates decline significantly with increasing ecological divergence (Fig. 6*C*), fitting predictions of an isolation-by-adaptation model (90). Negative genome-wide relationships between F_{ST} and f_d (Fig. 4 and *SI Appendix*, Fig. S12) further support the role of divergent selection in reproductive isolation, with the caveat that F_{ST} is sensitive to variation in within-population genetic diversity (101), and that elevated f_d reflects localized increases in diversity associated with introgression (8, 71). Ecological selection likely acts as a source of postzygotic isolation due to reduced hybrid fitness, as suggested by prior hybrid zone studies in rattlesnakes (50, 52, 53). However, it is also plausible that premating isolation due to local adaptation in divergent environments may act as a source of reinforcement in contact zones. Importantly, intrinsic incompatibilities and ecological divergence are not mutually exclusive in their effects on reproductive isolation. Instead, they are likely to have epistatic effects on fitness (102), such that modest increases in either intrinsic or ecological isolation can precipitate large reductions in gene flow as divergence progresses. Against a background of widespread selection against introgression, we also detect localized signals of adaptive introgression at loci underlying venom composition and immune function (Fig. 7), illustrating that hybridization can facilitate beneficial allele exchange even as genome-wide coupling strengthens reproductive isolation.

As discussed above, we find that recombination rate variation exerts a strong influence on the genomic landscape of introgression during speciation in rattlesnakes. Across most species pairs, effective migration rates are positively correlated with recombination rate (Fig. 4 and *SI Appendix*, Fig. S9), and the strength of this association increases with genetic divergence (Fig. 6*A*). Regions experiencing barrier effects are also found disproportionately in regions

of low recombination (Fig. 3 and *SI Appendix*, Figs. S7 and S21). Moreover, introgression landscapes are more tightly correlated between more divergent species pairs (Fig. 6*D* and *SI Appendix*, Figs. S17 and S18). These patterns support a central prediction of speciation theory: that the effects of selection against foreign alleles are amplified in genomic regions where recombination is reduced (Fig. 1), thereby strengthening the total barrier to gene flow through linkage disequilibrium (8, 9, 17, 103). Indeed, we suggest that the divergence-dependent increase in the correlation between introgression and recombination observed here (Fig. 6*A*) reflects an emergent property of genome-wide coupling across the speciation continuum, following the view that coupling reflects the buildup of genome-wide linkage disequilibrium (7, 9). Similar relationships between recombination and introgression have been reported across a wide range of taxa, including rabbits and house mice (19, 22), *Mimulus* monkeyflowers (23), *Xiphophorus* swordtails (21), *Heliconius* butterflies (8), *Bombus* bumblebees (104), *Quercus* oaks (105), and *Pogoniulus* tinkerbirds (106), underscoring the generality of recombination-mediated species barriers. However, few studies have examined these relationships explicitly across multiple scales of divergence within a single clade. Our findings in *Crotalus* provide a comparative demonstration that recombination rate is a key axis along which the genetic architecture of reproductive isolation is reorganized through coupling of species barriers.

A surprising result from our analyses is that rates of introgression also tend to increase in gene-rich regions of the rattlesnake genome (Fig. 4 and *SI Appendix*, Fig. S11). This pattern initially appears to contradict theoretical expectations that the strength of selection against gene flow is dependent on the density of selected sites, leading to stronger barriers in gene-rich regions [Fig. 1*B*; (8, 17)]. However, our results demonstrate that this signature arises due to mechanisms of fine-scale recombination, rather than reduced selection on genes. In snakes, meiotic recombination is concentrated in functional regions, resulting in elevated recombination rates in regions of high gene density (Fig. 5 *A* and *B*). Opposing theoretical effects of recombination and gene density therefore cannot be treated as completely independent predictors of introgression, but rather as interrelated features of genome organization with interacting effects. Indeed, we show that the relationship between gene density and introgression is strongly contingent on recombination rate (Fig. 5*D*), and that gene density has a tempering effect on introgression when this interaction is explicitly modeled (*SI Appendix*, Table S11). This is consistent with selection against foreign alleles in functional regions, but this effect is partially masked by the concentration of recombination in those same regions. The same qualitative pattern has been found independently in *Xiphophorus* swordtail fishes (21, 40), despite differences in molecular mechanisms directing the localization of recombination hotspots between lineages; recombination hotspots in snakes are directed at least in part by PRDM9 and in swordtails they are not (18, 21, 39, 61). Our findings indicate that associations between mechanisms of fine-scale recombination rate variation and genome organization can override simplified expectations for the genome-wide distribution of species barriers. More broadly, they emphasize the need for theoretical and empirical studies of speciation with gene flow to account not only for recombination rate per se, but also where recombination occurs relative to genes and regulatory elements. Accounting for such interactions provides a more realistic framework for predicting how genome organization shapes introgression landscapes during complex speciation with gene flow.

Our study presents compelling evidence that sex chromosomes play a substantial role in the transition from weakly differentiated populations to strongly isolated species during rattlesnake speciation. Rates of introgression are lower on the Z chromosome than autosomes between most species (Fig. 3 and *SI Appendix*, Fig. S8 and Table S5), barriers accumulate faster on the Z chromosome during divergence (Fig. 6*F*), and recurrent barrier loci are disproportionately Z-linked (*SI Appendix*, Table S17). Moreover, the Z chromosome exhibits a more rapid decrease in introgression across the speciation continuum than autosomes (Fig. 6*G* and *SI Appendix*, Fig. S20), suggesting that sex-linked regions are a nexus for accelerated coupling of barriers in the presence of gene flow. These patterns signal the presence of large Z-effects, wherein admixture of sex chromosomes disproportionately affects hybrid fitness (18, 85, 98, 107–109). Previous studies found evidence potentially consistent with large Z-effects in rattlesnakes, including reduced Z-linked heterozygosity and nucleotide diversity and elevated genetic differentiation relative to autosomes (18, 60, 110, 111). Evidence of large Z-effects based on these signatures is tentative, however, as they can arise through demographic processes and enhanced linked selection alone and may not necessarily translate to a direct role in reproductive isolation (84, 101, 112). However, a detailed analysis of the hybrid zone between *C. viridis* and *C. scutulatus* revealed steeper genomic clines and higher coupling coefficients on the Z chromosome relative to autosomes (50), providing more direct evidence that sex chromosomes contribute disproportionately to species barriers in secondary contact.

We extend these findings by demonstrating that Z-linked species barriers are not only more prevalent, but also emerge earlier than autosomal barriers as divergence increases, indicating a key role of the Z chromosome in the coupling of genome-wide barriers. The accelerated accumulation of Z-linked barriers in rattlesnakes aligns with empirical observations in model systems (e.g., refs. 113–115) and theoretical predictions that sex chromosomes are especially prone to rapid accumulation of hybrid incompatibilities due to exposure of deleterious recessive alleles to selection in the heterogametic sex, faster rates of molecular evolution, and sex-biased selective pressures (84, 116). Signal of large Z-effects may also relate to the potential presence of Haldane's rule in rattlesnakes [i.e., females suffer greater fitness costs of hybridization than males, (114, 117)] as well as special roles of sex-linked genes in adaptation to different environments. For example, the Z chromosome harbors expanded repertoires of chemosensory genes, including olfactory and vomeronasal receptors (118, 119), which are plausible targets of divergent ecological and sexual selection. Divergence at such loci may contribute to premating isolation through mate recognition and environmentally mediated chemical signaling at contact zones, and also through postzygotic isolation in the form of selection against hybrids. Directly testing these possibilities will require integrative analyses combining genomic, functional, and behavioral approaches, which will further reveal the degree to which Z-linked barriers in rattlesnakes reflect intrinsic incompatibilities, divergent ecological adaptation, and reinforcement.

In conclusion, tracing patterns of introgression across a continuum of divergence demonstrates how the genome-wide barrier to gene flow emerges and strengthens during complex speciation. Reproductive isolation in rattlesnakes is mediated by divergent selection among many loci and the combined roles of recombination and genome organization in shaping the coupling of species barriers, facilitating a key transition from genic to genomic phases of speciation (6, 9, 12). Our results further indicate an outsized role of sex chromosomes in speciation, with the Z chromosome exhibiting earlier, stronger, and more rapid barrier accumulation, likely acting as a catalyst in the evolution of genome-wide barrier effects. By investigating patterns of introgression in the context of the recombination landscape and functional annotation, our study presents an empirical framework for gaining a deeper understanding of how adaptation, intrinsic incompatibilities, and linkage disequilibrium shape the evolution of strong reproductive isolation during complex speciation with gene flow.

Materials and Methods

We assembled a reference genome for the Southwestern Speckled Rattlesnake (*C. pyrrhus*) using long-read and chromatin contact data. We performed gene and repeat annotation and used synteny between *C. pyrrhus* and *C. viridis* (60) and *C. adamanteus* (67) to assign scaffolds to chromosomes. We analyzed whole genome sequencing data for 181 *Crotalus* specimens (*SI Appendix*, Table S3), including 103 new samples and 78 from previous studies (18, 49, 50, 69, 87, 110, 111, 120). We mapped filtered reads to the *C. pyrrhus* reference genome using BWA mem (121), and called variants using GATK (122). We estimated the phylogeny of the Speckled and Western Rattlesnake species complexes using concatenated maximum likelihood, coalescent species tree inference, and phylogenetic networks. We estimated the demographic histories of *Crotalus* species using the sequentially Markov coalescent model implemented in SMC++ (123). We estimated recombination rates using pyrho (124), incorporating demographic history from SMC++ (124). We identified recombination hotspots following previous studies (18, 61). We calculated the admixture proportion [f_d; (71)] between 13 species pairs in nonoverlapping 1 Mb and 100 kb windows (*SI Appendix*, Fig. S6). We estimated d_{xy} and F_{ST} using pixy (125). We used patterns of linkage disequilibrium (r^2) and d_{xy} to distinguish introgression from incomplete lineage sorting. We tested relationships between f_d and recombination rate, exon density, and F_{ST} using linear models and calculated Spearman's correlation coefficients for each test based on mean values in nonoverlapping 1 Mb windows. We fit linear and nonlinear models to the relationship between the Spearman correlation coefficient between f_d and recombination rate and evolutionary divergence and to the relationship between f_d and evolutionary and ecological divergence. We assessed model fit using the Corrected Akaike Information Criterion. We also analyzed models after performing phylogenetic correction, following (114, 126). We used a permutation approach to identify outlier barrier windows with lower f_d than observed in null distributions. We performed bootstrapping to compare rates of introgression in focal regions linked to key adaptive traits and overrepresented biological processes in shared barriers to the genome background. Additional methods details are provided in *SI Appendix*.

Data, Materials, and Software Availability. Genomic data have been deposited in NCBI (PRJNA1460337, PRJNA593834, PRJNA1150930, and PRJNA1454467) (127–130). Some study data are available upon request (Precise sampling coordinates are omitted here to protect sensitive populations. Requests can be sent to drew.schield@virginia.edu.). The computational workflow and associated analysis scripts used in this work are available at https://github.com/kfarleigh/crotalus_introgression_wholegenome (131). All other data are included in the manuscript and/or supporting information.

ACKNOWLEDGMENTS. This work was supported by University of Virginia startup funds to D.R.S., NSF postdoctoral research fellowship DBI-2409958 to K.F., NSF Grants DEB-1655571 and IOS-2307044 to T.A.C. and S.P.M., NSF graduate research fellowship 2136515 to S.R.H., National Geographic Society Grant NGS-91224R-21 to M.J.M., J.L.S., M.B., G.C.G., C.L.P., and H.F.C., and an American Museum of Natural History Theodore Roosevelt Memorial Fund Grant to M.J.M. We thank Bryan Hughes, Robert Hansen, Chip Cochran, Emily Taylor, Joshua Parker, Samuel Kerwin, Hayley Crowell, Michael Hogan, Andrew Holycross, Marjorie Matocq, Chris Feldman, and Danny Nielsen for guidance and assistance in the field.

Author affiliations: [a]Department of Biology, University of Virginia, Charlottesville, VA 22903; [b]Department of Biology, University of Texas at Arlington, Arlington, TX 76019; [c]Department of Integrative Biology, University of South Florida, Tampa, FL 33620; [d]Department of Integrative Biology, Michigan State University, East Lansing, MI 48824; [e]Life Sciences Institute, University of Michigan, Ann Arbor, MI 48109; [f]Department of Ecology and Evolutionary Biology, University of Michigan, Ann Arbor, MI 48109; [g]Facultad de Ciencias Biológicas, Universidad Juárez del Estado de Durango, Gòmez Palacio, Durango 35019, México; [h]Herp.MX, Villa de Àlvarez, Colima 28970, México; [i]Department of Biological Sciences, Clemson University, Clemson, SC 29634; [j]Biology Department, University of South Alabama, Mobile, AL 36688; [k]Department of Biological Sciences, University of Northern Colorado, Greeley, CO 80639; and [l]Department of Biological Sciences, Tarleton State University, Stephenville, TX 76402

1. M. A. F. Noor, J. L. Feder, Speciation genetics: Evolving approaches. *Nat. Rev. Genet.* **7**, 851–861 (2006).
2. J. L. Feder, S. P. Egan, P. Nosil, The genomics of speciation-with-gene-flow. *Trends Genet.* **28**, 342–350 (2012).
3. M. Ravinet *et al.*, Interpreting the genomic landscape of speciation: A road map for finding barriers to gene flow. *J. Evol. Biol.* **30**, 1450–1477 (2017).
4. O. Seehausen *et al.*, Genomics and the origin of species. *Nat. Rev. Genet.* **153**, 176–192 (2014).
5. C. M. Smadja, R. K. Butlin, A framework for comparing processes of speciation in the presence of gene flow. *Mol. Ecol.* **20**, 5123–5140 (2011).
6. C. Wu, The genic view of the process of speciation. *J. Evol. Biol.* **14**, 851–865 (2001).
7. E. B. Dopman, K. L. Shaw, M. R. Servedio, R. K. Butlin, C. M. Smadja, Coupling of barriers to gene exchange: Causes and consequences. *Cold Spring Harb. Perspect. Biol.* **16**, a041432 (2024).
8. S. H. Martin, J. W. Davey, C. Salazar, C. D. Jiggins, Recombination rate variation shapes barriers to introgression across butterfly genomes. *PLoS Biol.* **17**, e2006288 (2019).
9. N. H. Barton, Multilocus clines. *Evolution* **37**, 454–471 (1983).
10. N. H. Barton, B. O. Bengtsson, The barrier to genetic exchange between hybridising populations. *Heredity* **57**, 357–376 (1986).
11. S. M. Flaxman, A. C. Wacholder, J. L. Feder, P. Nosil, Theoretical models of the influence of genomic architecture on the dynamics of speciation. *Mol. Ecol.* **23**, 4074–4088 (2014).
12. J. L. Feder *et al.*, Genome-wide congealing and rapid transitions across the speciation continuum during speciation with gene flow. *J. Hered.* **105**, 810–820 (2014).
13. S. H. Martin *et al.*, Genome-wide evidence for speciation with gene flow in *Heliconius* butterflies. *Genome Res.* **23**, 1817–1828 (2013).
14. Q. Rougemont *et al.*, Subtle introgression footprints at the end of the speciation continuum in a clade of *Heliconius* butterflies. *Mol. Biol. Evol.* **40**, msad166 (2023).
15. H. Shang *et al.*, Drivers of genomic landscapes of differentiation across a *Populus* divergence gradient. *Mol. Ecol.* **32**, 4348–4361 (2023).
16. M. Schweizer *et al.*, Parallel plumage colour evolution and introgressive hybridization in wheatears. *J. Evol. Biol.* **32**, 100–110 (2019).
17. S. Aeschbacher, J. P. Selby, J. H. Willis, G. Coop, Population-genomic inference of the strength and timing of selection against gene flow. *Proc. Natl. Acad. Sci. U.S.A.* **114**, 7061–7066 (2017).
18. D. R. Schield *et al.*, Snake recombination landscapes are concentrated in functional regions despite PRDM9. *Mol. Biol. Evol.* **37**, 1272–1294 (2020).
19. M. W. Nachman, B. A. Payseur, Recombination rate variation and speciation: Theoretical predictions and empirical results from rabbits and mice. *Philos. Trans. R. Soc. B, Biol. Sci.* **367**, 409–421 (2012).
20. E. Calfee *et al.*, Selective sorting of ancestral introgression in maize and teosinte along an elevational cline. *PLoS Genet.* **17**, e1009810 (2021).
21. M. Schumer *et al.*, Natural selection interacts with recombination to shape the evolution of hybrid genomes. *Science* **360**, 656–660 (2018).
22. V. Janoušek, P. Munclinger, L. Wang, K. C. Teeter, P. K. Tucker, Functional organization of the genome may shape the species boundary in the house mouse. *Mol. Biol. Evol.* **32**, 1208–1220 (2015).
23. Y. Brandvain, A. M. Kenney, L. Flagel, G. Coop, A. L. Sweigart, Speciation and introgression between *Mimulus nasutus* and *Mimulus guttatus*. *PLoS Genet.* **10**, e1004410 (2014).
24. M. R. Glasenapp, G. H. Pogson, Selection shapes the genomic landscape of introgressed ancestry in a pair of sympatric sea urchin species. *Genome Biol. Evol.* **16**, evae124 (2024).
25. S. H. Martin, C. D. Jiggins, Interpreting the genomic landscape of introgression. *Curr. Opin. Genet. Dev.* **47**, 69–74 (2017).
26. X.-Y. Chen *et al.*, Evolution of the correlated genomic variation landscape across a divergence continuum in the genus *Castanopsis*. *Mol. Biol. Evol.* **41**, msae191 (2024).
27. M. Petr, S. Pääbo, J. Kelso, B. Vernot, Limits of long-term selection against Neandertal introgression. *Proc. Natl. Acad. Sci. U.S.A.* **116**, 1639–1644 (2019).
28. C. S. Maxwell, V. E. Sepulveda, D. A. Turissini, W. E. Goldman, D. R. Matute, Recent admixture between species of the fungal pathogen *Histoplasma*. *Evol. Lett.* **2**, 210–220 (2018).
29. K. C. Teeter *et al.*, Genome-wide patterns of gene flow across a house mouse hybrid zone. *Genome Res.* **18**, 67–76 (2008).
30. C. Feng, J. Wang, A. Liston, M. Kang, Recombination variation shapes phylogeny and introgression in wild diploid strawberries. *Mol. Biol. Evol.* **40**, msad049 (2023).
31. N. H. Barton, The dynamics of hybrid zones. *Heredity* **43**, 341–359 (1979).
32. P. Nosil, D. J. Funk, D. Ortiz-Barrientos, Divergent selection and heterogeneous genomic divergence. *Mol. Ecol.* **18**, 375–402 (2009).
33. D. Schluter, Evidence for ecological speciation and its alternative. *Science* **323**, 737–741 (2009).
34. S. Via, Divergence hitchhiking and the spread of genomic isolation during ecological speciation-with-gene-flow. *Philos. Trans. R. Soc. Lond. B, Biol. Sci.* **367**, 451–460 (2012).
35. R. Riesch *et al.*, Transitions between phases of genomic differentiation during stick-insect speciation. *Nat. Ecol. Evol.* **1**, 1–13 (2017).
36. D. R. Schield *et al.*, Sexual selection promotes reproductive isolation in barn swallows. *Science* **386**, eadj8766 (2024).
37. B. M. Moran *et al.*, The genomic consequences of hybridization. *eLife* **10**, e69016 (2021).
38. G. Coop, X. Wen, C. Ober, J. K. Pritchard, M. Przeworski, High-resolution mapping of crossovers reveals extensive variation in fine-scale recombination patterns among humans. *Science* **319**, 1395–1398 (2008).
39. Z. Baker *et al.*, Repeated losses of PRDM9-directed recombination despite the conservation of PRDM9 across vertebrates. *eLife* **6**, e24133 (2017).
40. M. Schumer, R. Cui, D. L. Powell, G. G. Rosenthal, P. Andolfatto, Ancient hybridization and genomic stabilization in a swordtail fish. *Mol. Ecol.* **25**, 2661–2679 (2016).
41. A. P. Hendry, D. I. Bolnick, D. Berner, C. L. Peichel, Along the speciation continuum in sticklebacks. *J. Fish Biol.* **75**, 2000–2036 (2009).
42. C. Roux *et al.*, Shedding light on the grey zone of speciation along a continuum of genomic divergence. *PLoS Biol.* **14**, e2000234 (2016).
43. S. Stankowski, M. Ravinet, Defining the speciation continuum. *Evolution* **75**, 1256–1273 (2021).
44. M. E. Douglas, M. R. Douglas, G. W. Schuett, L. W. Porras, Evolution of rattlesnakes (Viperidae; Crotalus) in the warm deserts of western North America shaped by Neogene vicariance and Quaternary climate change. *Mol. Ecol.* **15**, 3353–3374 (2006).
45. S. M. Harrington, B. D. Hollingsworth, T. E. Higham, T. W. Reeder, Pleistocene climatic fluctuations drive isolation and secondary contact in the red diamond rattlesnake (*Crotalus ruber*) in Baja California. *J. Biogeogr.* **45**, 64–75 (2018).

46. J. M. Meik, J. W. Streicher, A. M. Lawing, O. Flores-Villela, M. K. Fujita, Limitations of climatic data for inferring species boundaries: Insights from speckled rattlesnakes. *PLoS ONE* **10**, e0131435 (2015).
47. D. R. Schield *et al.*, Incipient speciation with biased gene flow between two lineages of the Western Diamondback Rattlesnake (*Crotalus atrox*). *Mol. Phylogenet. Evol.* **83**, 213–223 (2015).
48. D. R. Schield *et al.*, Cryptic genetic diversity, population structure, and gene flow in the Mojave rattlesnake (*Crotalus scutulatus*). *Mol. Phylogenet. Evol.* **127**, 669–681 (2018).
49. D. R. Schield *et al.*, Allopatric divergence and secondary contact with gene flow: A recurring theme in rattlesnake speciation. *Biol. J. Linn. Soc.* **128**, 149–169 (2019).
50. Y. Z. Francioli *et al.*, Estimation of genome-wide coupling in rattlesnake hybrids provides insight into the process of speciation and its progress. *Nat. Commun.* **16**, 10242 (2025).
51. D. W. Maag *et al.*, Variation in defensive and exploratory behaviors across a rattlesnake (*Crotalus scutulatus* × *viridis*) hybrid zone in southwestern New Mexico. *Sci. Rep.* **15**, 11989 (2025).
52. Z. L. Nikolakis *et al.*, Evidence that genomic incompatibilities and other multilocus processes impact hybrid fitness in a rattlesnake hybrid zone. *Evolution* **76**, 2513–2530 (2022).
53. D. R. Schield *et al.*, Insight into the roles of selection in speciation from genomic patterns of divergence and introgression in secondary contact in venomous rattlesnakes. *Ecol. Evol.* **7**, 3951–3966 (2017).
54. C. F. Smith *et al.*, The best of both worlds? Rattlesnake hybrid zones generate complex combinations of divergent venom phenotypes that retain high toxicity. *Biochimie* **213**, 176–189 (2023).
55. G. Zancolli *et al.*, Is hybridization a source of adaptive venom variation in rattlesnakes? A test, using a *Crotalus scutulatus* × *viridis* hybrid zone in Southwestern New Mexico. *Toxins* **8**, 188 (2016).
56. N. L. Dowell *et al.*, Divergent haplotypes in two toxin gene complexes encode alternative venom types within rattlesnake species. *Curr. Biol.* **28**, 1016–1026.e4 (2018).
57. C. M. Harrison *et al.*, Using morphological, genetic, and venom analyses to present current and historic evidence of *Crotalus horridus* x *adamanteus* hybridization on Jekyll Island. *Ga. SE Nat.* **21**, 158–174 (2022).
58. E. A. Myers, Genome-wide data reveal extensive gene flow during the diversification of the western rattlesnakes (Viperidae: Crotalinae: *Crotalus*). *Mol. Phylogenet. Evol.* **165**, 107313 (2021).
59. E. A. Myers *et al.*, Phylogenomic discordance is driven by wide-spread introgression and incomplete lineage sorting during rapid species diversification within rattlesnakes (Viperidae: *Crotalus* and *Sistrurus*). *Syst. Biol.* **73**, 722–741 (2024).
60. D. R. Schield *et al.*, The origins and evolution of chromosomes, dosage compensation, and mechanisms underlying venom regulation in snakes. *Genome Res.* **29**, 590–601 (2019).
61. C. Hoge *et al.*, Patterns of recombination in snakes reveal a tug-of-war between PRDM9 and promoter-like features. *Science* **383**, eadj7026 (2024).
62. S. R. Goldberg, Reproduction in the speckled rattlesnake, *Crotalus mitchellii* (Serpentes: Viperidae). *Bull. South. Calif. Acad. Sci.* **99**, 101–101 (2000).
63. M. L. Holding, M. J. Margres, D. R. Rokyta, H. L. Gibbs, Local prey community composition and genetic distance predict venom divergence among populations of the Northern Pacific rattlesnake (*Crotalus oreganus*). *J. Evol. Biol.* **31**, 1513–1528 (2018).
64. S. P. Mackessy, Evolutionary trends in venom composition in the Western Rattlesnakes (*Crotalus viridis sensu lato*): Toxicity vs. tenderizers. *Toxicon* **55**, 1463–1474 (2010).
65. J. M. Meik, R. D. Babb, "*Crotalus pyrrhus:* Southwestern speckled rattlesnake" in *Snakes of Arizona*, A. T. Holycross, J. C. Mitchell, Eds. (ECO Publishing, 2020), pp. 588–599.
66. E. N. Taylor, D. F. DeNardo, "Hormones and reproductive cycles in snakes" in *Hormones and Reproduction of Vertebrates*, D. O. Norris, K. H. Lopez, Eds. (Academic Press, 2011), pp. 355–372.
67. M. P. Hogan *et al.*, The genetic regulatory architecture and epigenomic basis for age-related changes in rattlesnake venom. *Proc. Natl. Acad. Sci. U.S.A.* **121**, e2313440121 (2024).
68. J. M. Meik, S. Schaack, O. Flores-Villela, J. W. Streicher, Integrative taxonomy at the nexus of population divergence and speciation in insular speckled rattlesnakes. *J. Nat. Hist.* **52**, 989–1016 (2018).
69. J. M. Bernstein *et al.*, Disentangling a genome-wide mosaic of conflicting phylogenetic signals in Western Rattlesnakes. *Mol. Phylogenet. Evol.* **206**, 108309 (2025).
70. M. L. Holding, M. G. Sovic, T. J. Colston, H. L. Gibbs, The scales of coevolution: Comparative phylogeography and genetic demography of a locally adapted venomous predator and its prey. *Biol. J. Linn. Soc.* **132**, 297–317 (2021).
71. S. H. Martin, J. W. Davey, C. D. Jiggins, Evaluating the use of ABBA–BABA statistics to locate introgressed loci. *Mol. Biol. Evol.* **32**, 244–257 (2015).
72. R. E. Green *et al.*, A draft sequence of the Neandertal genome. *Science* **328**, 710–722 (2010).
73. B. Charlesworth, Measures of divergence between populations and the effect of forces that reduce variability. *Mol. Biol. Evol.* **15**, 538–543 (1998).
74. M. C. Whitlock, D. E. Mccauley, Indirect measures of gene flow and migration: FST≠1/(4Nm+1). *Heredity* **82**, 117–125 (1999).
75. S. M. Flaxman, J. L. Feder, P. Nosil, Genetic hitchhiking and the dynamic buildup of genomic divergence during speciation with gene flow. *Evolution* **67**, 2577–2591 (2013).
76. M. P. Schilling *et al.*, Transitions from single- to multi-locus processes during speciation with gene flow. *Genes* **9**, 274 (2018).
77. R. D. Aldridge, D. Duvall, Evolution of the mating season in the pitvipers of North America. *Herpetol. Monogr.* **16**, 1–25 (2002).
78. K. G. Ashton, Body size variation among mainland populations of the western rattlesnake (*Crotalus viridis*). *Evolution* **55**, 2523–2533 (2001).
79. S. R. Hirst *et al.*, Island biogeography and competition drive rapid venom complexity evolution across rattlesnakes. *Evolution* **79**, 1419–1432 (2025).
80. A. M. Lawing, J. M. Meik, P. D. Polly, Climate and competition shape species' borders: A study of the panamint (*Crotalus stephensi*) and speckled (*Crotalus mitchellii*) rattlesnakes. *ISRN Zool.* **2012**, 528745 (2012).
81. J. M. Meik, J. A. Watson, A. M. Lawing, J. W. Streicher, An evaluation of parapatric distributions among ecologically similar rattlesnakes (Viperidae: Crotalus) in North American warm deserts. *Biol. J. Linn. Soc.* **135**, 541–557 (2022).
82. J. M. Meik *et al.*, Climatic temperature and precipitation jointly influence body size in species of western rattlesnakes. *R. Soc. Open Sci.* **11**, 240345 (2024).
83. P. Nosil, S. P. Egan, D. J. Funk, Heterogeneous genomic differentiation between walking-stick ecotypes: "Isolation by adaptation" and multiple roles for divergent selection. *Evolution* **62**, 316–336 (2008).
84. B. Charlesworth, J. A. Coyne, N. H. Barton, The relative rates of evolution of sex chromosomes and autosomes. *Am. Nat.* **130**, 113–146 (1987).
85. J. A. Coyne, H. A. Orr, "Two rules of speciation" in *Speciation and Its Consequences*, D. Otte, J. A. Endler, Eds. (Sinauer Associates, Inc., 1989), pp. 180–207.
86. P. E. Bolton, S. Mathur, H. L. Gibbs, A multifaceted approach to identify disease response genes in the endangered massasauga rattlesnake. *J. Hered.* **117**, 383–394 (2025), 10.1093/jhered/esaf088.
87. M. J. Margres *et al.*, The tiger rattlesnake genome reveals a complex genotype underlying a simple venom phenotype. *Proc. Natl. Acad. Sci. U.S.A.* **118**, e2014634118 (2021).
88. M. A. Roseman *et al.*, Insights from the timber rattlesnake (*Crotalus horridus*) genome for MHC gene architecture and evolution in threatened rattlesnakes. *J. Hered.* **116**, 591–602 (2025).
89. R. Burri *et al.*, Linked selection and recombination rate variation drive the evolution of the genomic landscape of differentiation across the speciation continuum of Ficedula flycatchers. *Genome Res.* **25**, 1656–1665 (2015).
90. P. Nosil, *Ecological Speciation* (Oxford University Press, 2012).
91. S. Via, Natural selection in action during speciation. *Proc. Natl. Acad. Sci. U.S.A.* **106**, 9939–9946 (2009).
92. R. K. Butlin, C. M. Smadja, Coupling, reinforcement, and speciation. *Am. Nat.* **191**, 155–172 (2018).
93. J. L. Feder, P. Nosil, The efficacy of divergence hitchhiking in generating genomic islands during ecological speciation. *Evolution* **64**, 1729–1747 (2010).
94. J. A. Coyne, H. A. Orr, *Speciation* (Sinauer Associates, Inc., 2004).
95. S. Gourbière, J. Mallet, Are species real? The shape of the species boundary with exponential failure, reinforcement, and the "missing snowball". *Evolution* **64**, 1–24 (2010).
96. D. C. Presgraves, The molecular evolutionary basis of species formation. *Nat. Rev. Genet.* **11**, 175–180 (2010).
97. J. A. Coyne, The genetic basis of Haldane's rule. *Nature* **314**, 736–738 (1985).
98. D. C. Presgraves, Sex chromosomes and speciation in *Drosophila*. *Trends Genet.* **24**, 336–343 (2008).
99. D. B. Sloan, J. C. Havird, J. Sharbrough, The on-again, off-again relationship between mitochondrial genomes and species boundaries. *Mol. Ecol.* **26**, 2212–2236 (2017).
100. M. Tobler, N. Barts, R. Greenway, Mitochondria and the origin of species: Bridging genetic and ecological perspectives on speciation processes. *Integr. Comp. Biol.* **59**, 900–911 (2019).
101. T. E. Cruickshank, M. W. Hahn, Reanalysis suggests that genomic islands of speciation are due to reduced diversity, not reduced gene flow. *Mol. Ecol.* **23**, 3133–3157 (2014).
102. M. C. Whitlock, P. C. Phillips, F. B. G. Moore, S. J. Tonsor, Multiple fitness peaks and epistasis. *Annu. Rev. Ecol. Evol. Syst.* **26**, 601–629 (1995).
103. A. D. Cutter, B. A. Payseur, Genomic signatures of selection at linked sites: Unifying the disparity among species. *Nat. Rev. Genet.* **14**, 262–274 (2013).
104. M. J. Christmas *et al.*, Genetic barriers to historical gene flow between cryptic species of alpine bumblebees revealed by comparative population genomics. *Mol. Biol. Evol.* **38**, 3126–3143 (2021).
105. R. Fu *et al.*, Genome-wide analyses of introgression between two sympatric Asian oak species. *Nat. Ecol. Evol.* **6**, 924–935 (2022).
106. L. Rancilhac *et al.*, Introgression across narrow contact zones shapes the genomic landscape of phylogenetic variation in an African bird clade. *Syst. Biol.* **74**, 935–951 (2025).
107. J. A. Coyne, Genetics and speciation. *Nature* **355**, 511–515 (1992).
108. D. E. Irwin, Sex chromosomes and speciation in birds and other ZW systems. *Mol. Ecol.* **27**, 3831–3851 (2018).
109. D. C. Presgraves, Evaluating genomic signatures of "the large X-effect" during complex speciation. *Mol. Ecol.* **27**, 3822–3830 (2018).
110. D. R. Schield, B. W. Perry, Z. L. Nikolakis, S. P. Mackessy, T. A. Castoe, Population genomic analyses confirm male-biased mutation rates in snakes. *J. Hered.* **112**, 221–227 (2021).
111. D. R. Schield *et al.*, The roles of balancing selection and recombination in the evolution of rattlesnake venom. *Nat. Ecol. Evol.* **696**, 1367–1380 (2022).
112. J. E. Pool, R. Nielsen, Population size changes reshape genomic patterns of diversity. *Evolution* **61**, 3001–3006 (2007).
113. J. Kitano *et al.*, A role for a neo-sex chromosome in stickleback speciation. *Nature* **461**, 1079–1083 (2009).
114. J. A. Coyne, H. A. Orr, Patterns of speciation in *Drosophila*. *Evolution* **43**, 362–381 (1989).
115. A. D. Cutter, X exceptionalism in *Caenorhabditis* speciation. *Mol. Ecol.* **27**, 3925–3934 (2018).
116. R. P. Meisel, T. Connallon, The faster-X effect: Integrating theory and data. *Trends Genet.* **29**, 537–544 (2013).
117. J. Haldane, Sex ratio and unisexual sterility in hybrids animals. *J. Genet.* **12**, 101–109 (1922).
118. M. P. Hogan *et al.*, Life history and chromosome organization determine chemoreceptor gene expression in rattlesnakes. *J. Hered.* **116**, 617–631 (2025).
119. M. P. Hogan *et al.*, The chemosensory repertoire of the Eastern diamondback rattlesnake (*Crotalus adamanteus*) reveals complementary genetics of olfactory and vomeronasal-type receptors. *J. Mol. Evol.* **89**, 313–328 (2021).
120. S. S. Gopalan *et al.*, Diverse gene regulatory mechanisms alter rattlesnake venom gene expression at fine evolutionary scales. *Genome Biol. Evol.* **16**, evae110 (2024).
121. H. Li, R. Durbin, Fast and accurate short read alignment with Burrows–Wheeler transform. *Bioinformatics* **25**, 1754–1760 (2009).
122. A. McKenna *et al.*, The genome analysis toolkit: A MapReduce framework for analyzing next-generation DNA sequencing data. *Genome Res.* **20**, 1297–1303 (2010).
123. J. Terhorst, J. A. Kamm, Y. S. Song, Robust and scalable inference of population history from hundreds of unphased whole genomes. *Nat. Genet.* **49**, 303–309 (2017).
124. J. P. Spence, Y. S. Song, Inference and analysis of population-specific fine-scale recombination maps across 26 diverse human populations. *Sci. Adv.* **5**, eaaw9206 (2019).
125. K. L. Korunes, K. Samuk, Pixy: Unbiased estimation of nucleotide diversity and divergence in the presence of missing data. *Mol. Ecol. Resour.* **21**, 1359–1368 (2021).
126. J. Felsenstein, Phylogenies and the comparative method. *Am. Nat.* **125**, 1–15 (1985).
127. K. Farleigh *et al.*, Data from "Crotalus pyrrhus genome assembly." NCBI BioProject. https://www.ncbi.nlm.nih.gov/bioproject/PRJNA1460337/. Deposited 1 May 2026.
128. D. R. Schield *et al.*, Data from "Western Rattlesnake whole genome resequencing for recombination maps." NCBI BioProject. https://www.ncbi.nlm.nih.gov/bioproject/PRJNA593834/. Deposited 5 December 2019.
129. J. M. Bernstein *et al.*, Data from "Whole genomes reveal a mosaic of evolutionary history: A case study in rattlesnakes." NCBI BioProject. https://www.ncbi.nlm.nih.gov/bioproject/PRJNA1150930/. Deposited 22 August 2024.
130. K. Farleigh *et al.*, Data from "Whole genome sequencing of the Speckled and Western Rattlesnake species complexes." NCBI BioProject. https://www.ncbi.nlm.nih.gov/bioproject/PRJNA1454467/. Deposited 16 April 2026.
131. K. Farleigh *et al.*, Data from "crotalus_introgression_wholegenome". GitHub Repository. https://github.com/kfarleigh/crotalus_introgression_wholegenome. Accessed 7 May 2026.